16039 FEBRUARY 1981 ST2

JOURNAL OF THE STRUCTURAL DIVISION

EFFECTIVE WIND LOADS ON FLAT ROOFS

By Theodore Stathopoulos,[1] M. ASCE, David Surry,[2] and Alan G. Davenport,[3] M. ASCE

INTRODUCTION

At any location on the exterior of a structure, the wind-induced pressures (both positive and negative) are likely to be highly unsteady, and also to vary significantly from point to point. This is due to turbulence in the flow, and turbulence caused by flow separation from the sharp edges of the building. The scale of the resulting pressure fluctuations must then depend on both the building size and the size of the eddies in the oncoming wind. Since these pressure variations are not necessarily well-correlated either in time or in space, the peak loads affecting large areas would be expected to be less than the sum of the peak loads acting at individual points within such areas. Point loads are significant for the design of fasteners; however many other structural elements have tributary areas of significant size and thus their design should recognize this potential alleviation of load rather than conservatively assume full correlation between the peak loads.

Numerous wind tunnel experiments on models have been carried out in the past to determine appropriate design pressures, but until recently almost all of them have been performed under uniform steady-flow conditions. Such experiments often yield results considerably different from those observed in full scale. Modern boundary layer flow simulations have led to results in satisfactory agreement with full-scale measurements (see, e.g., Refs. 1 and 2); however even among these recent studies, many have been mainly confined to investigations of static wind forces.

[1]Asst. Prof., Centre for Building Studies, Concordia Univ., Montreal, Quebec, Canada.
[2]Assoc. Research Dir., Boundary Layer Wind Tunnel Lab., The Univ. of Western Ontario, London, Ontario, Canada.
[3]Dir., Boundary Layer Wind Tunnel Lab., The Univ. of Western Ontario, London, Ontario, Canada.

Note.—Discussion open until July 1, 1981. To extend the closing date one month, a written request must be filed with the Manager of Technical and Professional Publications, ASCE. Manuscript was submitted for review for possible publication on June 22, 1979. This paper is part of the Journal of the Structural Division, Proceedings of the American Society of Civil Engineers, ©ASCE, Vol. 107, No. ST2, February, 1981. ISSN 0044-8001/81/0002-0281/$01.00.

16039 EFFECTIVE WIND LOADS ON FLAT ROOFS

KEY WORDS: **Aerodynamics;** Codes; Correlation; **Design; Pressure; Roofs;** Spectra; Tributaries; **Wind loads**

ABSTRACT: An experimental investigation of wind-induced pressure loads acting on two square-plan flat-roofed model structures (50ft and 225ft high in full scale) is described. Measurements of mean, peak, and root mean square pressures acting on points and over larger roof areas have been made in turbulent boundary layer flow simulating wind over urban and open country terrains. Area loads on the roofs have been measured both by a pneumatic-averaging technique, and by using a large flush-diaphragm transducer. Correlation coefficients and spectra of effective pressure loads on various regions of the roofs are also presented. A significant overestimation of peak loads may occur for larger areas if full correlation of the worst point pressures acting over the area is assumed.

REFERENCE: Stathopoulos, Theodore, Surry, David, and Davenport, Alan G., "Effective Wind Loads on Flat Roofs," *Journal of the Structural Division*, ASCE, Vol. 107, No. ST2, **Proc. Paper 16039**, February, 1981, pp. 281-298

Roofs in particular are vulnerable to wind action, especially over local areas near windward edges and corners. Near these locations, large local suctions (negative pressures) may occur which tend to lift roofing elements. The dynamic characteristics of these wind forces and their effects on roofs have not received much attention, perhaps partially due to difficulties in measuring the fluctuating loads.

This paper describes wind tunnel measurements of pressures on points and on larger areas of flat-roofed buildings, and compares some of the results to current practice. Special emphasis has been given to the dynamic characteristics of the loading, as well as to the combined wind forces acting together on different roof regions. A novel application of pneumatically averaging the unsteady pressures acting on specific model areas has been used to define peak area loads for different roof regions. Parallel measurements using large diaphragm transducers set flush with the flat roof have verified this technique. Conventional point pressure measurements have also been made. The comparison of these

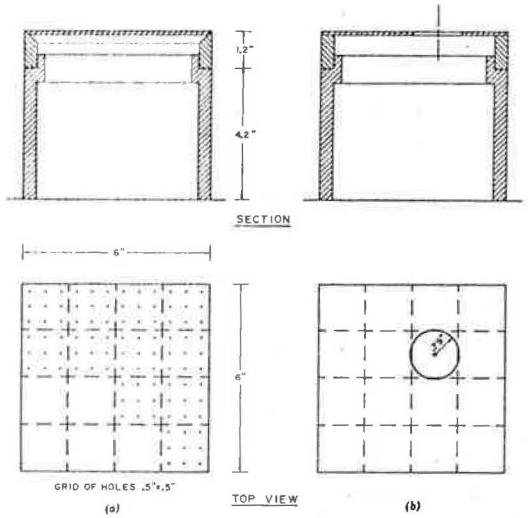

FIG. 1.—Sketch of Models: (*a*) With a Dense Grid of Pressure Holes; and (*b*) With Openings for Flush-Diaphragm Transducer

various experimental data stress the significance of the tributary area of assessment of the extreme wind loads acting on flat roofs. Furthermore, correlation coefficients and spectra for different roof areas help to give a picture of the development of the flow over the building, and therefore to determine some further characteristics of the random pressure loads. This paper is based on work reported in more detail in Ref. 10.

Experimental Measurements

All experiments were carried out at the University of Western Ontario's Boundary Layer Wind Tunnel Laboratory (BLWTL). The wind tunnel has a working section approx 80 ft × 8 ft (24 m × 2.5 m) wide, and has an adjustable

roof height averaging roughly 7 ft (2 m). Details of the wind tunnel are given by the third writer and Isyumov (4).

Two plexiglas models were used as sketched in Fig. 1. The first model has a regular distribution of pressure taps on the top for conventional measurements using pressure transducers with or without pneumatic averaging. The second model has a large-diameter, flush-diaphragm pressure transducer as part of the roof surface. The diaphragm area approximates 1/16 of the roof surface corresponding to the tributary area of nine pressure holes on the first model. The general arrangement of the measuring points was made so that, for wind perpendicular or at an angle of 45° to an edge, all roof areas could be investigated by using symmetry of flow and models. When using the flush-diaphragm transducer, only the inner roof region could be investigated. Each model is made of two parts. The top part includes the roof surface and can be used by itself to represent a low-rise building. The bottom part is a frame which, together with the top part, represents a taller building.

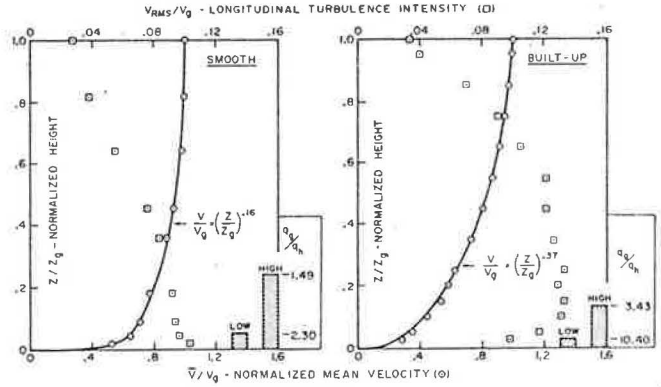

FIG. 2.—Vertical Profiles of Mean Velocity and Turbulence Intensity for Two Exposures

The models were mounted on the wind tunnel turntable which is located 80 ft (24 m) downstream from the bellmouth and 64 ft (19.5 m) away from the beginning of a random homogeneous roughness distribution. Two types of terrain were simulated. Open country terrain (the "smooth" case) was simulated using a carpet. The urban environment (the "built-up" case) was represented by a surface of approx 2-in. (50-mm) cubes distributed randomly. Typical velocity profiles are shown in Fig. 2. The free stream or gradient velocity, V_g, used in the wind tunnel was approx 45 fps (13.7 m/s).

Point-pressure instrumentation includes four 1/2-in. (13-mm) diaphragm strain-gage, differential-pressure transducers (Statham model PM 131TC) set in scanivalves under the turntable of the wind tunnel. Tubes [24 in. (610 mm) long and 1/16 in. (1.6 mm) in inside diameter] lead from the surface taps to the scanivalves. These tubes include damping constructions to keep the frequency response flat. The resulting system responds to pressure fluctuations on the model of up to about 100 Hz with negligible attenuation or distortion. Higher frequencies suffer increasing attenuation, although some response is obtained for signals of several hundred Hertz. Pressure measurements can be made in

parallel using several scanivalves, each of which is sampled at a rate of about 1,000 times/sec. Similar equipment, omitting the scanivalves, was also used to measure spatially-averaged pressures acting on roof areas, by interconnecting pneumatically an array of pressure taps through special multi-input manifolds. A detailed study of the response of these manifolds has been carried out (11). The inherent frequency response of the manifolded systems is similar to that of the component tubes, as presented in Ref. 11. For direct area measurements, a flush-diaphragm pressure transducer of the inductance type (Validyne model DP-104) mounted on the model was used. It has a resonance at 600 Hz, implying that its response up to 100 Hz is essentially flat. In all cases, differences between the pressure exerted on roof points or areas and the static pressure of the free stream were measured.

Digitization of the pressure signals and analysis of the data using a PDP-8/I digital computer on-line, gave the maximum, minimum, mean, and root mean square (RMS) pressures over a 60-sec period. The dynamic pressure of the flow above the boundary layer ($1/2\ \rho\ V_g^2$) was measured similarly, and used to determine pressure coefficients. Appropriate filtering and recording of the pressure signals coming from the various roof segments were carried out in order to allow correlation and spectral analysis of pressure loads, as detailed further in Ref. 10.

Scaling

For measurements of pressure loads on a rigid model, correct scaling requires the characteristics of the velocity profiles to be similar to full scale. Given this, the ratio of any length from the boundary layer to a characteristic length of the model determines the length scale. The velocity profiles of Fig. 2, taken at the location of the models without the models in place, yield a number of boundary layer characteristics for consideration. An exponential law $\bar{V}/V_g = (Z/Z_g)^a$, in which $\bar{V}$ = the mean velocity, at height Z; and a = an experimentally-determined constant, fits very well with most of the measured values. An alternate expression for the velocity profile near the surface is the logarithmic law $\bar{V}/V_g = (1/\kappa)\ C_g\ \ln\ (Z/Z_o)$. In this relationship, κ = von Karman's constant equal to 0.4; C_g^2 = a surface drag coefficient defined in terms of the surface shear stress τ_o as $C_g^2 = \tau_o/\rho\ V_g^2$; and Z_o = the roughness length, i.e., a quantity which characterizes the surface roughness elements, but is usually considerably smaller than their physical size. Typical values of these parameters for different full-scale terrains, taken from Ref. 5, are compared to those obtained from the measured velocity profiles in the wind tunnel in Table 1. The data indicate that a 1:500-length scale is appropriate. The corresponding full-scale dimensions of the models are shown in Table 2. Jensen and Franck's results (7) indicate that the experimental coefficients may well be representative for other length scales as well, as long as h/Z_o is maintained (h = the building height). Furthermore, their results indicate little sensitivity to scale changes of the order of 2 or so.

There is some flexibility in the selection of the velocity scale and consequently the time scale since $t_P/t_M = (L_P/L_M)(V_M/V_P)$, in which M and P signify model and prototype, respectively. The wind tunnel speed is chosen to provide acceptable signal to noise ratios. The velocity and time scales are then based

on the ratio of this speed to the full-scale wind speed of interest. In this case, this leads to velocity and time scales of about 3:10 and 1:150, respectively. Consequently, the experimental sampling rate corresponds to about 7 samples/sec/channel in full scale, and pressure fluctuations with frequencies up to about 0.7 Hz in full scale can be detected without distortion or attenuation.

The choice of sampling period is determined to be sufficiently long to provide statistically stable estimates of mean and RMS pressures and to ensure that measured maximum and minimum pressures provide representative estimates of peaks encountered during a full-scale interval of approx 1 h. The hourly average wind speed is a convenient, statistically-stable value which can straightforwardly be determined in full scale. The 60-sec sampling period used satisfies these requirements.

TABLE 1.—Velocity Profile Parameters for Full-Scale and Simulated Terrains

Exposure (1)	Z_g, in feet (2)	Z_o, in inches (3)	a (4)	C_g (5)
Full Scale				
Open country	900	0.4–4	0.16	0.042
Forest, suburban areas	1,300	12–40	0.28	0.044
City centers	1,700	40–200	0.40	0.046
Model Scale				
Smooth	1.83	0.01	0.16	0.042
Built-up	3.33	0.45	0.37	0.048

Note: 1 in. = 25.4 mm; and 1 ft = 305 mm.

TABLE 2.—Dimensions of Buildings in Wind Tunnel Experiments and in Full Scale

	Model Scale, in inches			Full Scale (1:500), in feet			h/Z_o	
Building (1)	Height (2)	Length (3)	Width (4)	Height (5)	Length (6)	Width (7)	Smooth (8)	Built-up (9)
Low	1.2	6.0	6.0	50	250	250	120.0	2.7
High	5.4	6.0	6.0	225	250	250	540.0	12.0

Note: 1 in. = 25.4 mm; and 1 ft = 305 mm.

Fastest-mile wind speeds are also often used as the reference speed for building codes. The relationship between fastest mile and hourly speeds can be determined as a function of the fastest-mile speed. For example Hollister (6) indicates that, for open country conditions the fastest-mile wind speed ≈1.29 (hourly mean speed) for wind speeds of design interest.

Pressure Coefficients

The maximum, minimum, mean, and RMS pressure coefficients for each individual roof point [see Fig. 1(*a*)] have been measured for the two different exposures described, two model buildings (low and high), and two wind directions (normal and oblique). The pressure coefficients are defined as

$$C_{p_{MAX}} = \frac{p_{MAX}}{q_h}, \; C_{p_{MIN}} = \frac{p_{MIN}}{q_h}, \; C_{\bar{p}} = \frac{\bar{p}}{q_h}, \; C_{p_{RMS}} = \frac{p_{RMS}}{q_h} \quad \ldots\ldots\ldots\ldots (1)$$

in which p_{MAX} = the maximum instantaneous pressure measured over the sampling period; p_{MIN} = the minimum instantaneous pressure measured over the sampling period; $\bar{p}$ = the temporal mean pressure; p_{RMS} = the RMS pressure = $\sqrt{(p-\bar{p})^2}$; and $q_h = 1/2\ \rho\ \bar{V}_h^2$ = the dynamic head associated with the hourly mean velocity at roof height $\bar{V}_h$. All pressures are differential pressures with respect to the static pressure at gradient height.

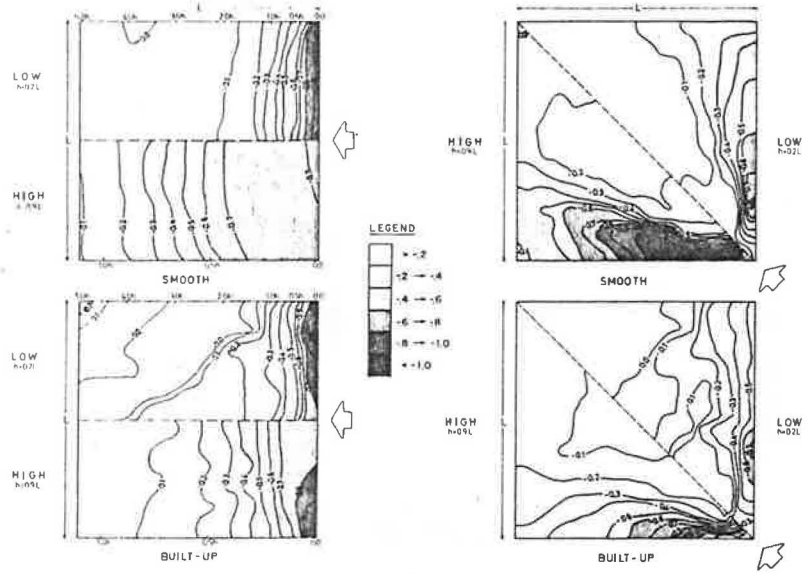

FIG. 3.—Local Mean Pressure Coefficients

During the experiment, it was more convenient to measure the pressure coefficients with respect to the dynamic pressure at gradient height. The conversion factors q_g/q_h have been determined from the velocity profiles of Fig. 2 and are included there.

Results: Local Pressure Coefficients

Contours of mean, peak, and RMS pressure coefficients for all parameter combinations considered are shown in Figs. 3, 4, and 5. Considering the symmetry of flow, contours are shown for each wind direction on half the roof only. However, it should be noted that the contour pattern is not absolutely symmetrical because of the random nature of the surface roughness, some local nonuniformity of the flow, and the natural statistical variability associated with such measurements.

Regarding mean pressure coefficients (see Fig. 3), it can be observed that there is almost always suction all over the roof. Regardless of exposure, the highest suction occurs near the windward edge of the roof and decreases from

there with increasing distance. There is some tendency for slightly higher suction coefficients for the smooth exposure in the case of 45° oblique wind flow. This has also been reported by Jensen and Franck (7) and others.

The comparison of mean pressure contours for the normal wind between high and low roofs under smooth exposure shows that reattachment of the mean flow occurs further from the leading edge for the higher roof. The result is that the front part of the lower roof supports a steeper pressure gradient and the rear half is under no substantial mean pressure load. The flow reattachment length is approximately a constant number of building heights. The built-up exposure results are similar, although local flow disturbances cloud the comparison a little.

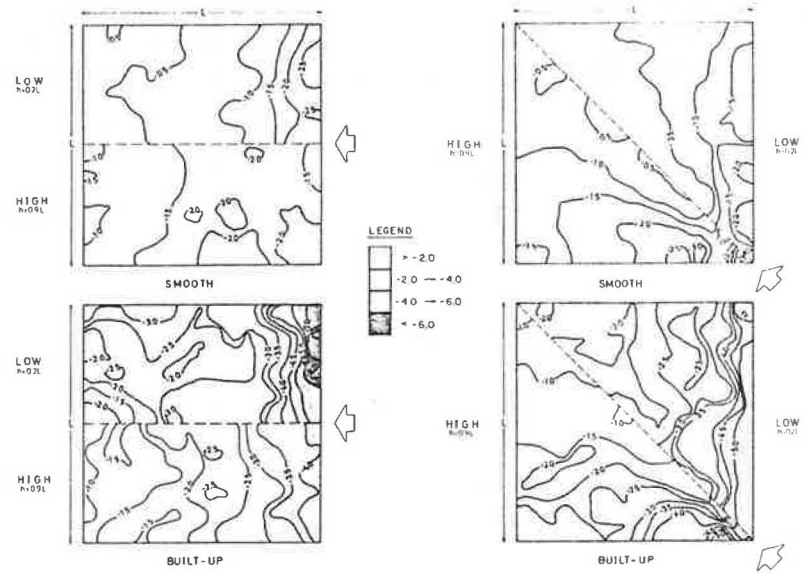

FIG. 4.—Local Negative Peak Pressure Coefficients

More severe pressure coefficients occur for wind directed towards the roof corner. The edges near the corner (but not at the very corners), are more heavily loaded than in the case of normal wind. This is consistent with the formation of vortices along the leading edges, which has been commonly observed by previous investigators.

The contours of uncorrelated negative peak instantaneous pressure coefficients are shown in Fig. 4. The general pattern appears disorganized, particularly for the built-up exposure. Although not shown, the peak positive pressure coefficients present a similar pattern, with magnitudes of the order of 0.6–0.9 for the smooth and 1.0–2.0 for the built-up exposure. The broad range of the peak fluctuations, more pronounced on the low roof for both wind directions, is very characteristic. Again, the most severe suctions are caused by the 45° oblique wind. Generally speaking, the extreme pressure coefficients on the high roof are either equal to or less severe than those on the low roof. (Keeping in mind, of course, that reference velocity pressures are higher for the higher root).

and those for the local and pneumatically-averaged technique were taken from experiments carried out several months apart under nominally the same conditions. Furthermore, different weighting functions are inherent in the two methods, the pneumatic technique being uniform, and the transducer being weighted

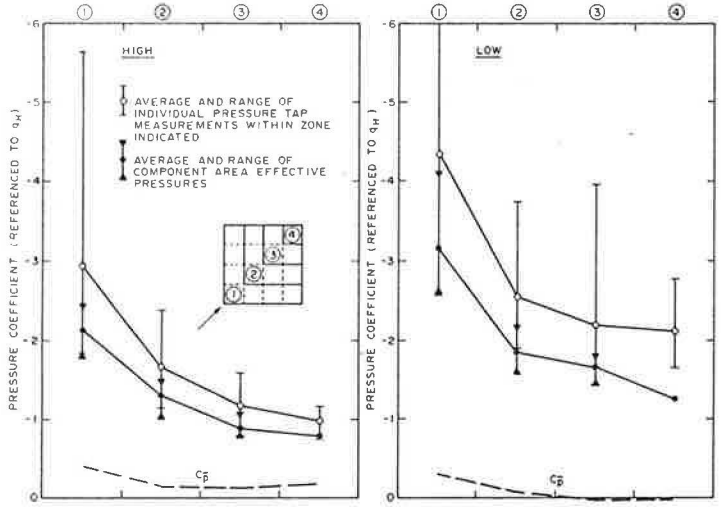

FIG. 8.—Comparison of Peak Suction Coefficients Derived from Local and Area Measurements (Built-up Exposure)

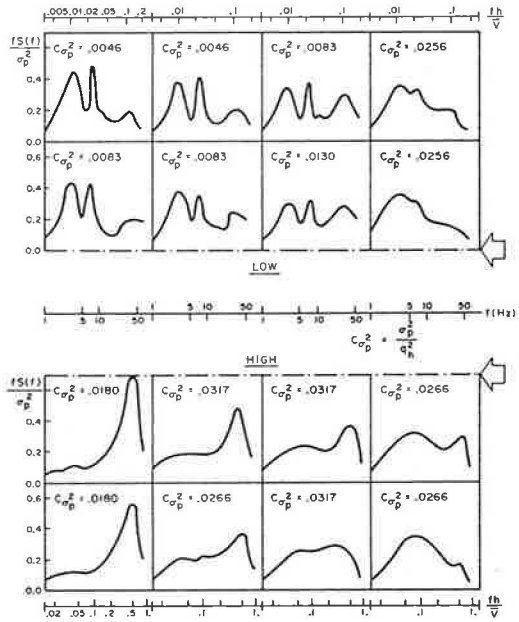

FIG. 9.—Spectra of Pressure Loads on All Roof Regions (Smooth Exposure, Normal Wind)

according to the deflection shape of the diaphragm.

The pneumatic-averaging technique has been used to assess peak area loads over a large part of the roof to illustrate the significance of the nonsimultaneous effect of the peak point pressures. Measurements were made for both exposures, both wind directions, and both models for all roof regions. Typical results are shown in Fig. 8 for an oblique wind acting on both the high and low roof. Both the local pressure coefficients, and the effective pressure coefficients for the component areas shown, have been averaged over the four zones as indicated, in the inset. Similar results are available (10) for the other wind direction/exposure combinations. In almost all cases, both the average and extreme limits of the noninstantaneous peak values given by the individual pressure taps are much more severe than the true spatially-averaged peaks. In some cases, the whole range of the spatially-averaged peaks is less than the range of individual extremes. Thus, a significant overestimation of the peak total load occurs when point pressures alone are used. The amount of overestimation increases with the proximity of the zone to the edge and appears to depend on the location of the roof area with regard to the wind direction.

It is interesting to note that Kim and Mehta (8) measured peak, mean, and RMS loads on a flat roof in a full-scale experiment and determined a probabilistic model for predicting the peak loads from the measured mean and RMS values. They applied this model successfully using the results of the present study (10); i.e., their measured peak pressure coefficients are predicted from the measured mean and RMS pressure coefficients of the current study, despite the different geometries of the present models and the full-scale building.

Spectra and Correlation Coefficients for Roof Component Areas

Since this study was primarily aimed at the characteristics of the effective pressures acting on roof areas rather than points, the pneumatic-averaging technique has also been used to determine spectra of pressure loads affecting the 16 equal-sized regions. Representative results are presented in Fig. 9. Each power spectral density function of pressure load is drawn in the appropriate area. All spectra are normalized by the variance, the values of which are also indicated, in coefficient form, normalized by the square of the dynamic pressure at roof height. The spectra can be classified into two different, although not clearly separated regions, i.e., the windward region and the wake region.

The pressure spectra in the windward region of the roof are similar to the spectrum of longitudinal turbulence which can be described by the universal equation suggested by the third writer (3). According to this expression, the maximum energy of the wind turbulence in full scale is associated with the lower wave numbers (peak at $f/\bar{V} \approx 4.6 \times 10^{-4}$ cycles/ft $= 1.5 \times 10^{-3}$ cycles/m), which corresponds to the low frequency peak, at about $f/\bar{V} \approx 1.4 \times 10^{-3}$ cycles/m, of the measured spectra in equivalent full-scale units. This accumulation of energy at low frequencies is clearly shown in the windward regions for all cases. It is interesting to compare these results with the information given by Kramer and Gerhardt (9) for power spectral densities of pressure loads on a flat roof. Although their geometry was not the same, the spectrum given in Ref. 9 for normal wind agrees in shape and intensity to the spectra obtained for the windward regions in this study, the main difference being

that Kramer and Gerhardt's peak occurs at higher frequencies centered on an equivalent full-scale value of $f/\bar{V} \approx 3 \times 10^{-3}$ cycles/m. Note, however; that the spectra presented here correspond to area loading, whereas Kramer and Gerhardt's are for point pressures. Furthermore, Kramer and Gerhardt's length scaling within the boundary layer was somewhat relaxed and could account for the apparent shift in the energy to higher frequencies. Fig. 9 also indicates

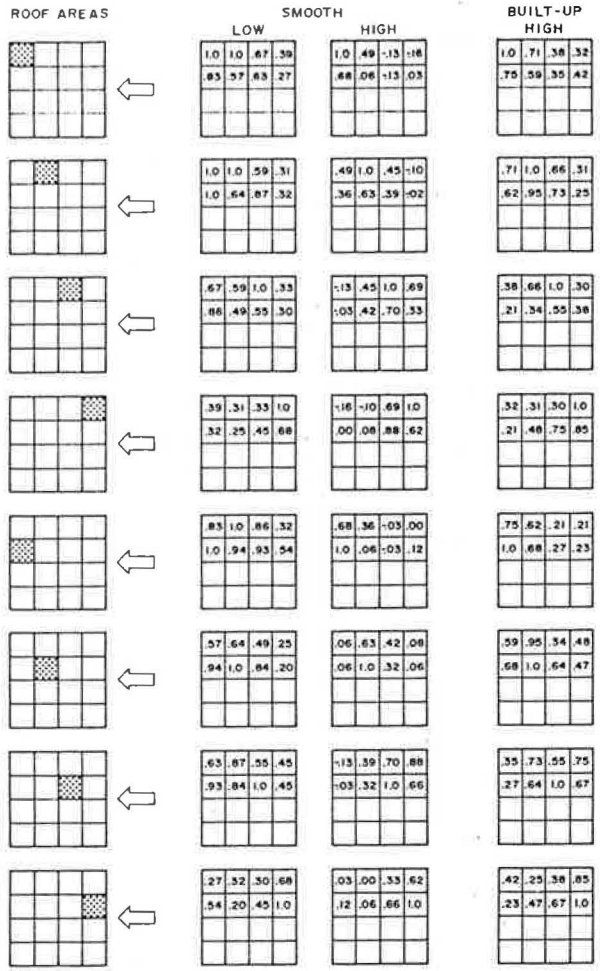

FIG. 10.—Pressure Correlation Coefficients for Various Roof Regions

that two other energy peaks become more pronounced towards the downwind side of the roof, reaching their maximum value in the wake region. The highest of these energy peaks is centered on ~3 Hz ($fh/\bar{V} \approx 0.01$) for the low and ~40 Hz ($fh/\bar{V} \sim 0.45$) for the high model (model scale frequencies). Whereas the response to the gustiness of the wind can be seen over the entire roof on the low model, it only affects the first windward zone of the high model.

This may be due to the greater displacement of the shear layer above the higher model.

Since the effective pressures acting on the subregions of the roof retain a considerable amount of the dynamic nature of the point pressures, it is necessary to define the cross correlations or cross spectra between different roof areas in order to determine the unsteady load acting on still larger parts of the structural system of the roof extending over more than 1/16 of the area. The effectiveness of the dynamic wind loads experienced by large structural elements is thus further reduced. The loss of correlation between two points, which is beneficial for the roof loading, depends on their position and the distance between them.

Correlation coefficients between the area loads on the different regions of the low and high roof are shown in Fig. 10 for different exposures and normal wind. Each zone of Fig. 10 gives the correlation coefficients between the associated shaded area and all the others. The following observations can be made:

1. The height of the roof and the roughness of the exposure are very important factors in the development of high or low correlations. Negative correlation coefficients have been found only in the case of the high model for the smooth exposure wind and are small. Generally, the correlation coefficients change more rapidly for the higher roof and more gradually for the built-up exposure. This may be due to the larger components of roof load dependent on the wind turbulence in the latter case, partially due to the more severe gustiness, and partially due to the closer proximity of the shear layer to the roof.
2. Although the correlation coefficients are expected to decay with increasing separation between the various subareas (the rate of decrease depending on the position of the two subareas, as related to the wind flow direction), this does not always happen. There are cases in which the correlation of the pressure load is higher with a more remote zone of the roof than with a neighboring region. No clear explanation is available; however in some cases it appears to be associated with the reattachment of the separated shear layer.
3. With respect to the wind flow direction, the correlation coefficients (10) appear higher for regions located in the trace of the vortices developed over the roof for the 45° oblique wind direction.

Results of cross-spectral analysis show that, in most cases, the quad-spectra are insignificant; this implies that the out-of-phase components of the pressure load fluctations are negligible. The co-spectra given in Ref. 10 indicate that the pressure load fluctuations are strongly correlated for small separations; thus the co-spectral densities appear fairly comparable to the power spectral densities for adjacent regions, particularly at low frequencies.

Assessment of Effective Wind Loads on Large Roof Subsections

The spectra of pressure loads acting on the 1/16 sections of the roof were used to derive spectra of the total fluctuating wind force acting on larger sections of the roofs. Results were obtained for sections made up of multiples of the 1/16-square areas under the various conditions of exposure, wind direction, and height of roof (10). Typical cases for force spectra acting on a roof quarter

for an oblique wind and different combinations of height and exposure are presented in Fig. 11. Also shown are mean square effective pressure coefficients, found by numerical integration. These coefficients are of the same form as defined in Fig. 9.

In general, the variance coefficients are smaller for larger areas, although they may be higher for the larger area than for some of their component areas if the larger area includes components on the windward side of the roof. It is also interesting to note that larger spectral peaks appear for the lower roof. No clear explanation of this fact is available at present, but the observation indicates that lower roofs may be more susceptible to resonant effects.

Comparison of Local Pressure Coefficient Results with Codes and Standards

Since pressure coefficients are determined with respect to different reference speeds in various countries, it is very difficult to make comparisons directly between coefficients. Instead, a simple illustrative comparison is made in terms of pressure acting on the roofs of a low and a higher building, similar to those used in this study, according to the specifications of the 1977 Commentary to the National Building Code of Canada (NBCC) (simple method), the American National Standard Institute (ANSI A58.1-1972), and the present results. The comparison in summarized in Fig. 12 which shows both the actual pressures, and ratios normalized by the current experimental results. Ratios greater than 1.0 imply code conservatism. The wind speed considered corresponds to an hourly average of 60 mph at 30 ft over an open country exposure. Considering a similar storm system, i.e., the same gradient height speed over a densely built-up urban environment, the corresponding hourly average speed at 30 ft would be only 23 mph. Since the simple method of the NBCC does not recognize any terrain differences, the same values are specified for both exposures.

The ANSI refers all pressure coefficients to the fastest mile speed at roof height. Conversion of the hourly average of 60 mph to a fastest mile of 77 mph was made by using Hollister's charts (6). Different values of velocity pressures (which include gust effects) are specified for different exposures.

To determine the pressures from the present study, the wind speed at roof height was calculated using the experimental velocity profiles of Fig. 2. The pressure coefficients used from the experimental study are the worst peak suction coefficients measured at any point in the area considered, and thus do not include any alleviation associated with spatial averaging. This comparison was adopted because the areas used in these experiments do not conveniently aline with the divisions of roof areas considered in the NBCC or ANSI standard.

The comparison shows that the NBCC significantly overestimates the pressure loads, in particular for the corner region, the built-up terrain, and the lower building. The results suggest some adjustment should be made for the edge and corner specified coefficients which are very high, and that allowance for a rougher exposure in the simple method of the Canadian Code might be worthwhile. The ANSI also significantly overestimates the negative pressures on the perimeter zones; however the ANSI appears to underestimate some of the local loads in the interior of the roof, particularly for the higher building and the rougher terrain. This is likely to be compensated by spatial averaging as per Figs. 6 and 8.

Examination of the measured pressures reveals that generally the dynamic component predominates. Codes usually overestimate the mean loads and underestimate the gust factors. For example, the NBCC considerably overestimates the mean (by factors of 1.5 and up), whereas the gust factors found experimentally were typically in the range 2–7.5 compared to the value of 2.5

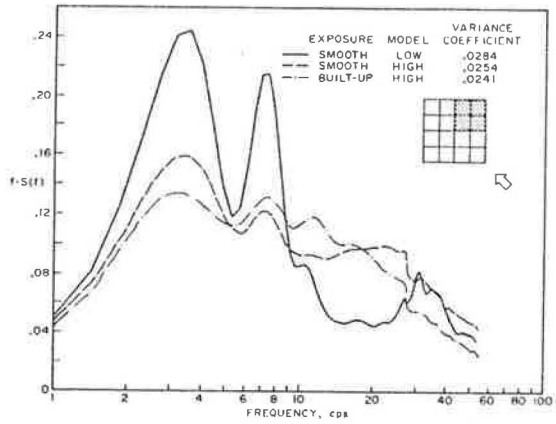

FIG. 11.—Spectra of Pressure Loads Acting on a Roof Quarter

CAVEAT: PRESSURE VALUES DO NOT INCLUDE ANY RESONANT EFFECT

		Peak Wind Pressures In psf and As Ratios of Those Found in the Present Study											
EXPOSURE =		Smooth (NBCC: A; ANSI: C)						Built-up (NBCC: C; ANSI: A)					
REGION =		R		W		C		R		W		C	
		psf	ratio	psf	ratio	psf	ratio	psf	ratio	psf	ratio	psf	ratio
NBCC	Low	-26.7	1.17	-53.2	1.87	-79.7	2.80	-26.7	2.68	-53.2	3.02	-79.7	4.53
	High	-36.2	0.98	-72.5†	1.57†	-109.0†	1.96†	-36.2	1.52	-72.5†	2.67†	-109.0†	3.21†
ANSI	Low	-18.9	0.83	-64.8	2.27	-135.0	4.74	-7.0	0.71	-24.0	1.36	-50.0	2.84
	High	-25.2	0.68	-86.4	1.87	-180.0	3.24	-13.3	0.56	-45.6	1.68	-95.0	2.79
Present Study	Low	-22.8	1.00	-28.5	1.00	-28.5	1.00	-9.9	1.00	-17.6	1.00	-17.6	1.00
	High	-37.0	1.00	-46.2	1.00	-55.5	1.00	-23.8	1.00	-27.2	1.00	-34.0	1.00

Note: 1 psf = 47.9 N/m^2
1 ft. = 305 mm.

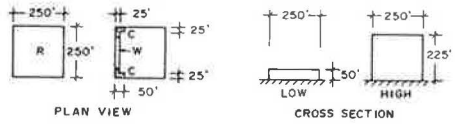

† under the provisions of the 1980 NBCC, for taller buildings the coefficients specified for C are reduced by a factor of 0.67 and for W by a factor of 0.75. Similar reductions have also been effected for low-rise buildings.

FIG. 12.—NBCC, ANSI, and Comparative Experimental Values

specified by the Code. These large experimental gust factors may be particularly significant if the structural response of all or part of the roof is susceptible to dynamic effects. It should be noted that since the experimental coefficients used in the aforementioned comparisons are local values, spatial averaging will further reduce the loads appropriate for overall structural considerations. This

is recognized in the NBCC for the design of primary structural systems only (reduction of gust factor from 2.5 to 2.0), and in the ANSI for areas greater than 200 sq ft (18.6 m^2).

During the course of preparation of this paper, both the NBCC and ANSI have been undergoing revision. The ANSI revised coefficients have not been examined in detail, although they appear to be somewhat reduced while still remaining conservative. Some indication of the 1980 NBCC changes have been added to Fig. 12. For taller buildings, the roof corner and roof edge coefficients have been reduced so that for a smooth exposure the experimental ratios quoted are reduced to about 1.2–1.3. For low-rise buildings, the 1980 Code has introduced significant changes. These include: the specification of peak coefficients (i.e., they inherently include a gust factor); revision of the coefficients to more closely reflect the most recent experimental data (see Refs. 12, 13, and 14); reduction in load coefficients for increasing tributary area; and specification of completely separate coefficients appropriate to the design of the primary wind-resisting structural system. The effect of terrain roughness has not been introduced into the simple method of the Code; however the reference wind pressure now reduces with height down to 6 m rather than the previous value of 10 m.

Conclusions

The following conclusions can be made:

1. The wind-induced pressures acting on a flat roof have a major dynamic component.
2. A significant overestimation of the wind load acting on roof areas occurs when the lack of spatial correlation of gusts is not taken into account. This overestimation is higher for areas more heavily loaded and increases with the area size.
3. Even within the aforementioned conservative comparison, based entirely on local pressure coefficients, the 1977 Commentary to the Canadian Code overestimates the suctions acting on a flat roof, in particular for the lower roof and the rougher exposure considered. The ANSI A58.1-1972 document underestimates some of the interior zone local loads (which may be compensated by spatial averaging), but significantly overestimates the suctions on the roof perimeter.

Acknowledgments

The writers would like to acknowledge the assistance, encouragement, and advice provided by their colleagues at the BLWTL. The helpful suggestion of the Validyne transducer as the most appropriate instrument for the purpose was made by R. D. Marshall of the National Bureau of Standards, of the United States. Financial support for this project was provided by the National Research Council of Canada.

Appendix I.—References

1. Apperley, L., Surry, D., Stathopoulos, T., and Davenport, A. G., "Comparative Measurements of Wind Pressure on a Model of the Full-Scale Experimental House at Aylesbury, England," *Journal of Industrial Aerodynamics*, Vol. 4, Nos. 2 and 3, Aug., 1979, pp. 207–227.
2. Dalgliesh, W. A., "Comparison of Model/Full-Scale Wind Pressures on a High-Rise Building," *Journal of Industrial Aerodynamics*, Vol. 1, No. 1, June, 1975, pp. 55–66.
3. Davenport, A. G., "The Spectrum of Horizontal Gustiness Near the Ground in High Winds," *Quarterly Journal of the Royal Meteorological Society*, Vol. 87, No. 372, April, 1961, pp. 194–211.
4. Davenport, A. G., and Isyumov, N., "The Application of the Boundary Layer Wind Tunnel to the Prediction of Wind Loading," presented at the 1967 Symposium of Wind Effects on Buildings and Structures, held at Ottawa, Canada.
5. Davenport, A. G., et al., "New Approaches to Design Against Wind Action," seminar sponsored by the ASCE Committee on Continuing Education (Preliminary Notes published by the Boundary Layer Wind Tunnel Laboratory, The University of Western Ontario, London, Canada).
6. Hollister, S. C., "The Engineering Interpretation of Weather Bureau Records for Wind Loading on Structures," presented at the Jan. 27–28, 1969, Technical Meeting Concerning Wind Loads on Buildings and Structures, held at the National Bureau of Standards, Gaithersburg, Md.
7. Jensen, M., and Franck, N., *Model-Scale Tests in Turbulent Wind*, Part II, The Danish Technical Press, Copenhagen, Denmark, 1965.
8. Kim, S. I., and Mehta, K. C., *Wind Loads on Flat Roof Area Through Full-Scale Experiment*, Institute for Disaster Research and Department of Civil Engineering, Texas Tech University, Lubbock, Tex., Sept., 1977.
9. Kramer, C., and Gerhardt, H. J., "WindKräfte auf Flachen und Wenig Geneigten Dachflächen," presented at the Jan. 21–22, 1976, 2. Kolloquium über Industrieaerodynamik, held at Aachen, West Germany.
10. Stathopoulos, T., "Wind Pressure Loads on Flat Roofs," thesis presented to the University of Western Ontario, in London, Ontario, Canada, in 1976, in partial fulfillment of the requirements for the degree of Master of Engineering Science.
11. Surry, D., and Stathopoulos, T., "An Experimental Approach to the Economical Measurement of Spatially Average Wind Loads," *Journal of Industrial Aerodynamics*, Vol. 2, No. 4, Jan., 1978, pp. 385–397.
12. Davenport, A. G., Surry, D., and Stathopoulos, T., "Wind Loads on Low Rise Buildings: Final Report of Phases I and II—Parts 1 and 2," *BLWT Report SS8-1977*, The University of Western Ontario, London, Ontario, Canada, Nov., 1977.
13. Davenport, A. G., Surry, D., and Stathopoulos, T., "Wind Loads on Low Rise Buildings: Final Report of Phase III—Parts 1 and 2," *BLWT-SS4-1978*, The University of Western Ontario, London, Ontario, Canada, July, 1978.
14. Surry, D., Stathopoulos, T., and Davenport, A. G., "The Wind Loading of Low Rise Buildings," *Proceedings of Canadian Structural Engineering Conference*, (Canadian Steel Industries Construction Council), 1978.

Appendix II.—Notation

The following symbols are used in this paper:

A = area of each elementary square region of the roof;
a = power law exponent;
C_g = square root of surface drag coefficient;
C_p = pressure coefficient;
f = frequency;
h = building height;
L = length;
p = pressure;
q_g = dynamic head at gradient height;
q_h = dynamic head at height h;
t = time;

$\vec{V}$ = mean velocity;
V_g = mean wind velocity at gradient height;
Z = height above ground;
Z_o = roughness length;
Z_g = gradient height;
κ = von Karman's constant;
ρ = air density;
σ_p = RMS pressure acting on each square region; and
τ_o = surface shear stress.

16039 EFFECTIVE WIND LOADS ON FLAT ROOFS

KEY WORDS: **Aerodynamics; Codes; Correlation; Design; Pressure; Roofs; Spectra; Tributaries; Wind loads**

ABSTRACT: An experimental investigation of wind-induced pressure loads acting on two square-plan flat-roofed model structures (50ft and 225ft high in full scale) is described. Measurements of mean, peak, and root mean square pressures acting on points and over larger roof areas have been made in turbulent boundary layer flow simulating wind over urban and open country terrains. Area loads on the roofs have been measured both by a pneumatic-averaging technique, and by using a large flush-diaphragm transducer. Correlation coefficients and spectra of effective pressure loads on various regions of the roofs are also presented. A significant overestimation of peak loads may occur for larger areas if full correlation of the worst point pressures acting over the area is assumed.

REFERENCE: Stathopoulos, Theodore, Surry, David, and Davenport, Alan G., "Effective Wind Loads on Flat Roofs," *Journal of the Structural Division*, ASCE, Vol. 107, No. ST2, Proc. Paper 16039, February, 1981, pp. 281-298

16039 FEBRUARY 1981 ST2

JOURNAL OF THE STRUCTURAL DIVISION

EFFECTIVE WIND LOADS ON FLAT ROOFS

By Theodore Stathopoulos,[1] M. ASCE, David Surry,[2] and Alan G. Davenport,[3] M. ASCE

INTRODUCTION

At any location on the exterior of a structure, the wind-induced pressures (both positive and negative) are likely to be highly unsteady, and also to vary significantly from point to point. This is due to turbulence in the flow, and turbulence caused by flow separation from the sharp edges of the building. The scale of the resulting pressure fluctuations must then depend on both the building size and the size of the eddies in the oncoming wind. Since these pressure variations are not necessarily well-correlated either in time or in space, the peak loads affecting large areas would be expected to be less than the sum of the peak loads acting at individual points within such areas. Point loads are significant for the design of fasteners; however many other structural elements have tributary areas of significant size and thus their design should recognize this potential alleviation of load rather than conservatively assume full correlation between the peak loads.

Numerous wind tunnel experiments on models have been carried out in the past to determine appropriate design pressures, but until recently almost all of them have been performed under uniform steady-flow conditions. Such experiments often yield results considerably different from those observed in full scale. Modern boundary layer flow simulations have led to results in satisfactory agreement with full-scale measurements (see, e.g., Refs. 1 and 2); however even among these recent studies, many have been mainly confined to investigations of static wind forces.

[1] Asst. Prof., Centre for Building Studies, Concordia Univ., Montreal, Quebec, Canada.
[2] Assoc. Research Dir., Boundary Layer Wind Tunnel Lab., The Univ. of Western Ontario, London, Ontario, Canada.
[3] Dir., Boundary Layer Wind Tunnel Lab., The Univ. of Western Ontario, London, Ontario, Canada.

Note.—Discussion open until July 1, 1981. To extend the closing date one month, a written request must be filed with the Manager of Technical and Professional Publications, ASCE. Manuscript was submitted for review for possible publication on June 22, 1979. This paper is part of the Journal of the Structural Division, Proceedings of the American Society of Civil Engineers, ©ASCE, Vol. 107, No. ST2, February, 1981. ISSN 0044-8001/81/0002-0281/$01.00.

Roofs in particular are vulnerable to wind action, especially over local areas near windward edges and corners. Near these locations, large local suctions (negative pressures) may occur which tend to lift roofing elements. The dynamic characteristics of these wind forces and their effects on roofs have not received much attention, perhaps partially due to difficulties in measuring the fluctuating loads.

This paper describes wind tunnel measurements of pressures on points and on larger areas of flat-roofed buildings, and compares some of the results to current practice. Special emphasis has been given to the dynamic characteristics of the loading, as well as to the combined wind forces acting together on different roof regions. A novel application of pneumatically averaging the unsteady pressures acting on specific model areas has been used to define peak area loads for different roof regions. Parallel measurements using large diaphragm transducers set flush with the flat roof have verified this technique. Conventional point pressure measurements have also been made. The comparison of these

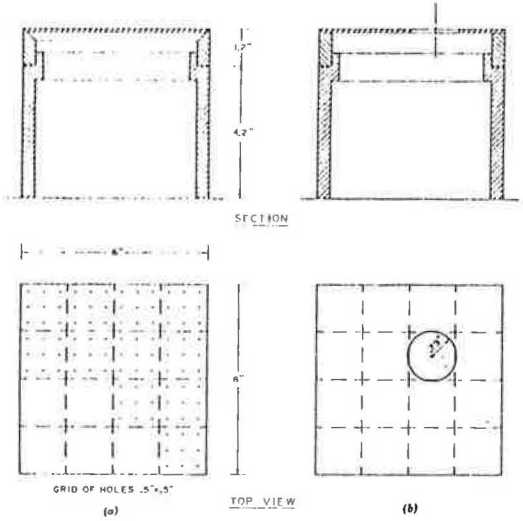

FIG. 1.—Sketch of Models: (*a*) With a Dense Grid of Pressure Holes; and (*b*) With Openings for Flush-Diaphragm Transducer

various experimental data stress the significance of the tributary area of assessment of the extreme wind loads acting on flat roofs. Furthermore, correlation coefficients and spectra for different roof areas help to give a picture of the development of the flow over the building, and therefore to determine some further characteristics of the random pressure loads. This paper is based on work reported in more detail in Ref. 10.

Experimental Measurements

All experiments were carried out at the University of Western Ontario's Boundary Layer Wind Tunnel Laboratory (BLWTL). The wind tunnel has a working section approx 80 ft × 8 ft (24 m × 2.5 m) wide, and has an adjustable

roof height averaging roughly 7 ft (2 m). Details of the wind tunnel are given by the third writer and Isyumov (4).

Two plexiglas models were used as sketched in Fig. 1. The first model has a regular distribution of pressure taps on the top for conventional measurements using pressure transducers with or without pneumatic averaging. The second model has a large-diameter, flush-diaphragm pressure transducer as part of the roof surface. The diaphragm area approximates 1/16 of the roof surface corresponding to the tributary area of nine pressure holes on the first model. The general arrangement of the measuring points was made so that, for wind perpendicular or at an angle of 45° to an edge, all roof areas could be investigated by using symmetry of flow and models. When using the flush-diaphragm transducer, only the inner roof region could be investigated. Each model is made of two parts. The top part includes the roof surface and can be used by itself to represent a low-rise building. The bottom part is a frame which, together with the top part, represents a taller building.

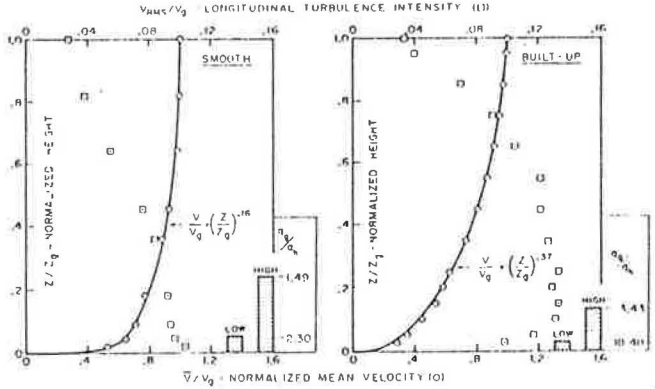

FIG. 2.—Vertical Profiles of Mean Velocity and Turbulence Intensity for Two Exposures

The models were mounted on the wind tunnel turntable which is located 80 ft (24 m) downstream from the bellmouth and 64 ft (19.5 m) away from the beginning of a random homogeneous roughness distribution. Two types of terrain were simulated. Open country terrain (the "smooth" case) was simulated using a carpet. The urban environment (the "built-up" case) was represented by a surface of approx 2-in. (50-mm) cubes distributed randomly. Typical velocity profiles are shown in Fig. 2. The free stream or gradient velocity, V_g, used in the wind tunnel was approx 45 fps (13.7 m/s).

Point-pressure instrumentation includes four 1/2-in. (13-mm) diaphragm strain-gage, differential-pressure transducers (Statham model PM 131TC) set in scanivalves under the turntable of the wind tunnel. Tubes [24 in. (610 mm) long and 1/16 in. (1.6 mm) in inside diameter] lead from the surface taps to the scanivalves. These tubes include damping constructions to keep the frequency response flat. The resulting system responds to pressure fluctuations on the model of up to about 100 Hz with negligible attenuation or distortion. Higher frequencies suffer increasing attenuation, although some response is obtained for signals of several hundred Hertz. Pressure measurements can be made in

parallel using several scanivalves, each of which is sampled at a rate of about 1,000 times/sec. Similar equipment, omitting the scanivalves, was also used to measure spatially-averaged pressures acting on roof areas, by interconnecting pneumatically an array of pressure taps through special multi-input manifolds. A detailed study of the response of these manifolds has been carried out (11). The inherent frequency response of the manifolded systems is similar to that of the component tubes, as presented in Ref. 11. For direct area measurements, a flush-diaphragm pressure transducer of the inductance type (Validyne model DP-104) mounted on the model was used. It has a resonance at 600 Hz, implying that its response up to 100 Hz is essentially flat. In all cases, differences between the pressure exerted on roof points or areas and the static pressure of the free stream were measured.

Digitization of the pressure signals and analysis of the data using a PDP-8/I digital computer on-line, gave the maximum, minimum, mean, and root mean square (RMS) pressures over a 60-sec period. The dynamic pressure of the flow above the boundary layer ($1/2\ \rho\ V_g^2$) was measured similarly, and used to determine pressure coefficients. Appropriate filtering and recording of the pressure signals coming from the various roof segments were carried out in order to allow correlation and spectral analysis of pressure loads, as detailed further in Ref. 10.

Scaling

For measurements of pressure loads on a rigid model, correct scaling requires the characteristics of the velocity profiles to be similar to full scale. Given this, the ratio of any length from the boundary layer to a characteristic length of the model determines the length scale. The velocity profiles of Fig. 2, taken at the location of the models without the models in place, yield a number of boundary layer characteristics for consideration. An exponential law $\bar{V}/V_g = (Z/Z_g)^a$, in which $\bar{V}$ = the mean velocity, at height Z; and a = an experimentally-determined constant, fits very well with most of the measured values. An alternate expression for the velocity profile near the surface is the logarithmic law $\bar{V}/V_g = (1/\kappa)\ C_g\ \ln\ (Z/Z_o)$. In this relationship, κ = von Karman's constant equal to 0.4; C_g^2 = a surface drag coefficient defined in terms of the surface shear stress τ_o as $C_g^2 = \tau_o/\rho\ V_g^2$; and Z_o = the roughness length, i.e., a quantity which characterizes the surface roughness elements, but is usually considerably smaller than their physical size. Typical values of these parameters for different full-scale terrains, taken from Ref. 5, are compared to those obtained from the measured velocity profiles in the wind tunnel in Table 1. The data indicate that a 1:500-length scale is appropriate. The corresponding full-scale dimensions of the models are shown in Table 2. Jensen and Franck's results (7) indicate that the experimental coefficients may well be representative for other length scales as well, as long as h/Z_o is maintained (h = the building height). Furthermore, their results indicate little sensitivity to scale changes of the order of 2 or so.

There is some flexibility in the selection of the velocity scale and consequently the time scale since $t_P/t_M = (L_P/L_M)(V_M/V_P)$, in which M and P signify model and prototype, respectively. The wind tunnel speed is chosen to provide acceptable signal to noise ratios. The velocity and time scales are then based

on the ratio of this speed to the full-scale wind speed of interest. In this case, this leads to velocity and time scales of about 3:10 and 1:150, respectively. Consequently, the experimental sampling rate corresponds to about 7 samples/sec/channel in full scale, and pressure fluctuations with frequencies up to about 0.7 Hz in full scale can be detected without distortion or attenuation.

The choice of sampling period is determined to be sufficiently long to provide statistically stable estimates of mean and RMS pressures and to ensure that measured maximum and minimum pressures provide representative estimates of peaks encountered during a full-scale interval of approx 1 h. The hourly average wind speed is a convenient, statistically-stable value which can straightforwardly be determined in full scale. The 60-sec sampling period used satisfies these requirements.

TABLE 1.—Velocity Profile Parameters for Full-Scale and Simulated Terrains

Exposure (1)	Z_g, in feet (2)	Z_o, in inches (3)	a (4)	C_g (5)
Full Scale				
Open country	900	0.4–4	0.16	0.042
Forest, suburban areas	1,300	12–40	0.28	0.044
City centers	1,700	40–200	0.40	0.046
Model Scale				
Smooth	1.83	0.01	0.16	0.042
Built-up	3.33	0.45	0.37	0.048

Note: 1 in. = 25.4 mm; and 1 ft = 305 mm.

TABLE 2.—Dimensions of Buildings in Wind Tunnel Experiments and in Full Scale

	Model Scale, in inches			Full Scale (1:500), in feet			h/Z_o	
Building (1)	Height (2)	Length (3)	Width (4)	Height (5)	Length (6)	Width (7)	Smooth (8)	Built-up (9)
Low	1.2	6.0	6.0	50	250	250	120.0	2.7
High	5.4	6.0	6.0	225	250	250	540.0	12.0

Note: 1 in. = 25.4 mm; and 1 ft = 305 mm.

Fastest-mile wind speeds are also often used as the reference speed for building codes. The relationship between fastest mile and hourly speeds can be determined as a function of the fastest-mile speed. For example Hollister (6) indicates that, for open country conditions the fastest-mile wind speed ≈1.29 (hourly mean speed) for wind speeds of design interest.

Pressure Coefficients

The maximum, minimum, mean, and RMS pressure coefficients for each individual roof point [see Fig. 1(*a*)] have been measured for the two different exposures described, two model buildings (low and high), and two wind directions (normal and oblique). The pressure coefficients are defined as

$$C_{p_{MAX}} = \frac{p_{MAX}}{q_h}, \; C_{p_{MIN}} = \frac{p_{MIN}}{q_h}, \; C_{\bar{p}} = \frac{\bar{p}}{q_h}, \; C_{p_{RMS}} = \frac{p_{RMS}}{q_h} \quad \ldots\ldots\ldots\ldots (1)$$

in which p_{MAX} = the maximum instantaneous pressure measured over the sampling period; p_{MIN} = the minimum instantaneous pressure measured over the sampling period; $\bar{p}$ = the temporal mean pressure; p_{RMS} = the RMS pressure = $\sqrt{(p - \bar{p})^2}$; and $q_h = 1/2\ \rho\ \bar{V}_h^2$ = the dynamic head associated with the hourly mean velocity at roof height $\bar{V}_h$. All pressures are differential pressures with respect to the static pressure at gradient height.

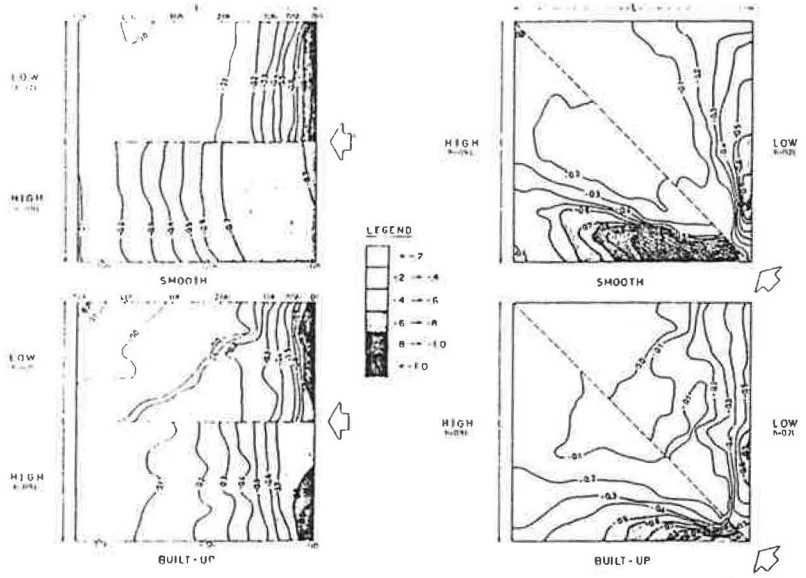

FIG. 3.—Local Mean Pressure Coefficients

During the experiment, it was more convenient to measure the pressure coefficients with respect to the dynamic pressure at gradient height. The conversion factors q_g/q_h have been determined from the velocity profiles of Fig. 2 and are included there.

Results: Local Pressure Coefficients

Contours of mean, peak, and RMS pressure coefficients for all parameter combinations considered are shown in Figs. 3, 4, and 5. Considering the symmetry of flow, contours are shown for each wind direction on half the roof only. However, it should be noted that the contour pattern is not absolutely symmetrical because of the random nature of the surface roughness, some local nonuniformity of the flow, and the natural statistical variability associated with such measurements.

Regarding mean pressure coefficients (see Fig. 3), it can be observed that there is almost always suction all over the roof. Regardless of exposure, the highest suction occurs near the windward edge of the roof and decreases from

there with increasing distance. There is some tendency for slightly higher suction coefficients for the smooth exposure in the case of 45° oblique wind flow. This has also been reported by Jensen and Franck (7) and others.

The comparison of mean pressure contours for the normal wind between high and low roofs under smooth exposure shows that reattachment of the mean flow occurs further from the leading edge for the higher roof. The result is that the front part of the lower roof supports a steeper pressure gradient and the rear half is under no substantial mean pressure load. The flow reattachment length is approximately a constant number of building heights. The built-up exposure results are similar, although local flow disturbances cloud the comparison a little.

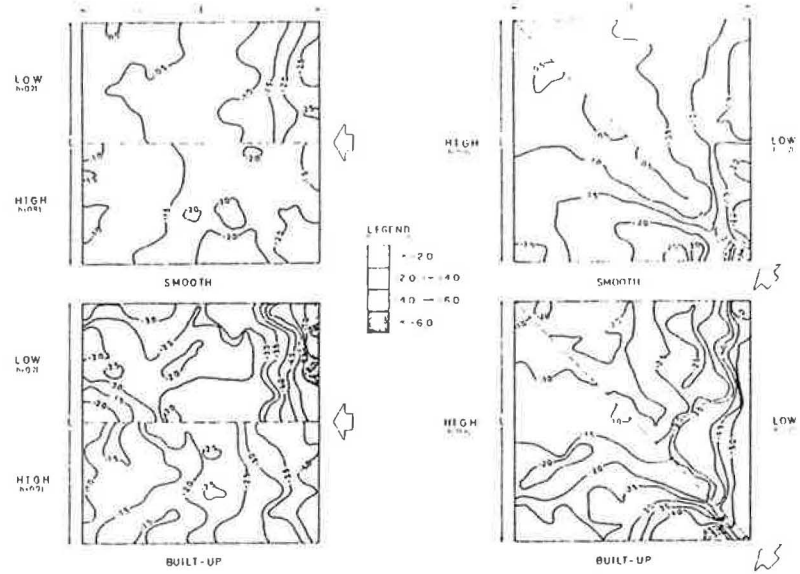

FIG. 4.—Local Negative Peak Pressure Coefficients

More severe pressure coefficients occur for wind directed towards the roof corner. The edges near the corner (but not at the very corners), are more heavily loaded than in the case of normal wind. This is consistent with the formation of vortices along the leading edges, which has been commonly observed by previous investigators.

The contours of uncorrelated negative peak instantaneous pressure coefficients are shown in Fig. 4. The general pattern appears disorganized, particularly for the built-up exposure. Although not shown, the peak positive pressure coefficients present a similar pattern, with magnitudes of the order of 0.6-0.9 for the smooth and 1.0-2.0 for the built-up exposure. The broad range of the peak fluctuations, more pronounced on the low roof for both wind directions, is very characteristic. Again, the most severe suctions are caused by the 45° oblique wind. Generally speaking, the extreme pressure coefficients on the high roof are either equal to or less severe than those on the low roof. (Keeping in mind, of course, that reference velocity pressures are higher for the higher roof).

Kramer and Gerhardt (9) present contours of pressure coefficients for a 45° wind acting on a cube-shaped building a little different from the high model described here. Their results are similar to the peak instantaneous suction coefficients shown in Fig. 4; however it is uncertain as to whether the coefficients in the two cases are strictly comparable in terms of the reference pressure and the relevant averaging times.

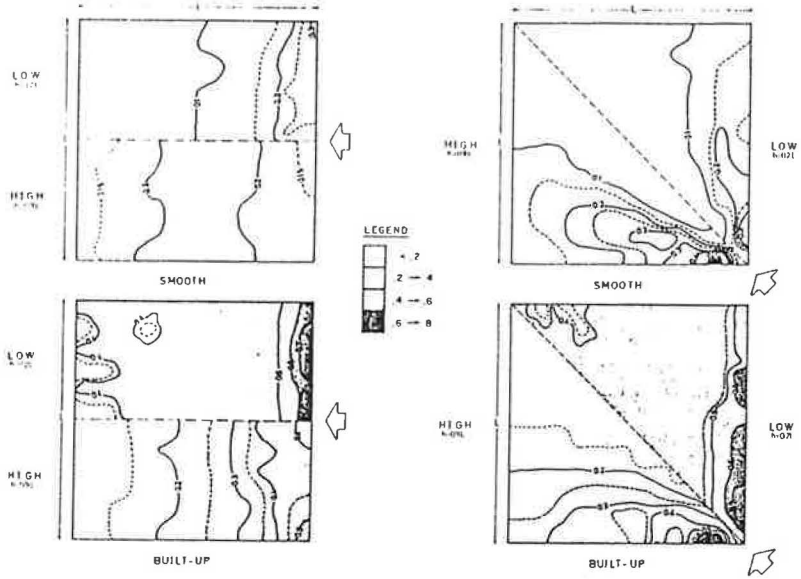

FIG. 5.—Local RMS Pressure Coefficients

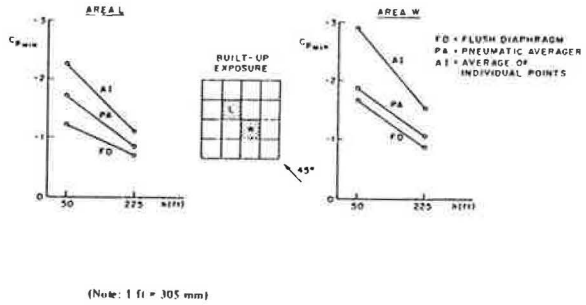

(Note: 1 ft = 305 mm)

FIG. 6.—Peak Suction Coefficients from Different Measurement Techniques

Fig. 5 shows the RMS pressure coefficient contours which provide a measure of the spread of the pressure fluctuations around the mean value. As expected, the RMS pressure coefficients have much larger values for the built-up exposure. The larger RMS values occur close to the windward edges of the roof and generally decrease downstream.

Results: Spatially-Averaged Pressure Coefficients

In order to study the influence of the tributary area and the nonsimultaneous effect of the local peak pressures, experiments with flush-diaphragm transducers covering specific roof regions were carried out. Measurements were also made by pneumatically averaging the pressures from taps corresponding to these regions. For these group measurements the roof was divided into the 16 equal square regions shown in Fig. 1(*a*). Each contains nine pressure taps. The round flush-diaphragm transducer covers an area corresponding virtually to the circle inscribed in each square area. The fact that the corners of each region are not covered by the sensitive part of the instrument is not expected to introduce significant errors, particularly for the interior regions where it was used.

Although not shown here, mean pressure coefficients obtained from the manifolding technique agree very well with those derived by averaging the mean values from the individual pressure taps (10). For peak areas loads, Fig. 6

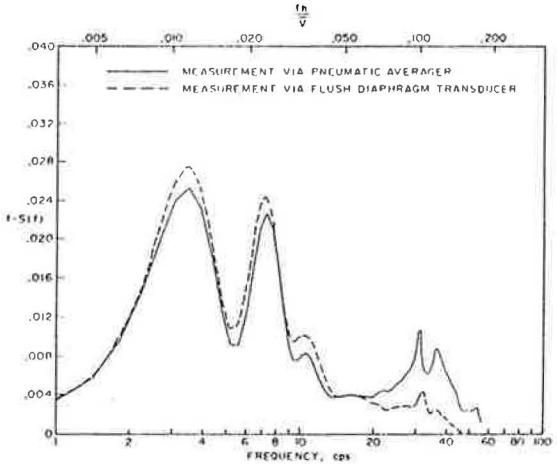

FIG. 7.—Comparison of Spectra from Different Measurement Techniques (Smooth Exposure, Low Model, Oblique Wind, Inner Region)

compares minimum pressure coefficients for inner roof regions obtained from flush-diaphragm transducer measurements, the average of the individual local peak measurements (assuming complete correlation), and the pneumatically-averaged results. This comparison indicates that the pneumatically-averaged results compare well with those of the direct area measurements of the flush-diaphragm transducer although they are always high. This is due in part to the overestimation of the high-frequency components, as shown by the comparative spectra of Fig. 7. The overestimation physically arises when the area over which the pressure fluctuations are coherent becomes much less than the tributary area associated with a single tap in the grid. This phenomenon has been examined by a simple heuristic analysis described in Ref. 10, and is subject to analytical correction if required. Generally, the resulting overestimation is conservative. Note that the differences apparent in Fig. 6 may not be solely due to this high frequency effect. They may arise from the fact that the data for the transducer

and those for the local and pneumatically-averaged technique were taken from experiments carried out several months apart under nominally the same conditions. Furthermore, different weighting functions are inherent in the two methods, the pneumatic technique being uniform, and the transducer being weighted

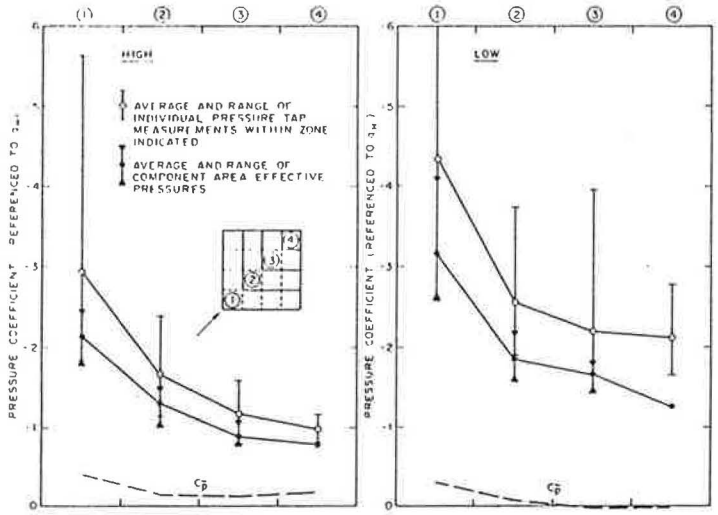

FIG. 8.—Comparison of Peak Suction Coefficients Derived from Local and Area Measurements (Built-up Exposure)

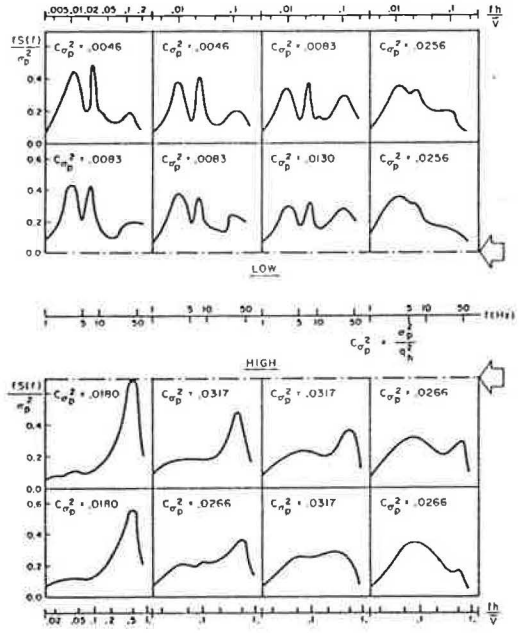

FIG. 9.—Spectra of Pressure Loads on All Roof Regions (Smooth Exposure, Normal Wind)

according to the deflection shape of the diaphragm.

The pneumatic-averaging technique has been used to assess peak area loads over a large part of the roof to illustrate the significance of the nonsimultaneous effect of the peak point pressures. Measurements were made for both exposures, both wind directions, and both models for all roof regions. Typical results are shown in Fig. 8 for an oblique wind acting on both the high and low roof. Both the local pressure coefficients, and the effective pressure coefficients for the component areas shown, have been averaged over the four zones as indicated, in the inset. Similar results are available (10) for the other wind direction/exposure combinations. In almost all cases, both the average and extreme limits of the noninstantaneous peak values given by the individual pressure taps are much more severe than the true spatially-averaged peaks. In some cases, the whole range of the spatially-averaged peaks is less than the range of individual extremes. Thus, a significant overestimation of the peak total load occurs when point pressures alone are used. The amount of overestimation increases with the proximity of the zone to the edge and appears to depend on the location of the roof area with regard to the wind direction.

It is interesting to note that Kim and Mehta (8) measured peak, mean, and RMS loads on a flat roof in a full-scale experiment and determined a probabilistic model for predicting the peak loads from the measured mean and RMS values. They applied this model successfully using the results of the present study (10); i.e., their measured peak pressure coefficients are predicted from the measured mean and RMS pressure coefficients of the current study, despite the different geometries of the present models and the full-scale building.

Spectra and Correlation Coefficients for Roof Component Areas

Since this study was primarily aimed at the characteristics of the effective pressures acting on roof areas rather than points, the pneumatic-averaging technique has also been used to determine spectra of pressure loads affecting the 16 equal-sized regions. Representative results are presented in Fig. 9. Each power spectral density function of pressure load is drawn in the appropriate area. All spectra are normalized by the variance, the values of which are also indicated, in coefficient form, normalized by the square of the dynamic pressure at roof height. The spectra can be classified into two different, although not clearly separated regions, i.e., the windward region and the wake region.

The pressure spectra in the windward region of the roof are similar to the spectrum of longitudinal turbulence which can be described by the universal equation suggested by the third writer (3). According to this expression, the maximum energy of the wind turbulence in full scale is associated with the lower wave numbers (peak at $f/\bar{V} \approx 4.6 \times 10^{-4}$ cycles/ft $= 1.5 \times 10^{-3}$ cycles/m), which corresponds to the low frequency peak, at about $f/\bar{V} \approx 1.4 \times 10^{-3}$ cycles/m, of the measured spectra in equivalent full-scale units. This accumulation of energy at low frequencies is clearly shown in the windward regions for all cases. It is interesting to compare these results with the information given by Kramer and Gerhardt (9) for power spectral densities of pressure loads on a flat roof. Although their geometry was not the same, the spectrum given in Ref. 9 for normal wind agrees in shape and intensity to the spectra obtained for the windward regions in this study, the main difference being

that Kramer and Gerhardt's peak occurs at higher frequencies centered on an equivalent full-scale value of $f/\bar{V} \approx 3 \times 10^{-1}$ cycles/m. Note, however; that the spectra presented here correspond to area loading, whereas Kramer and Gerhardt's are for point pressures. Furthermore, Kramer and Gerhardt's length scaling within the boundary layer was somewhat relaxed and could account for the apparent shift in the energy to higher frequencies. Fig. 9 also indicates

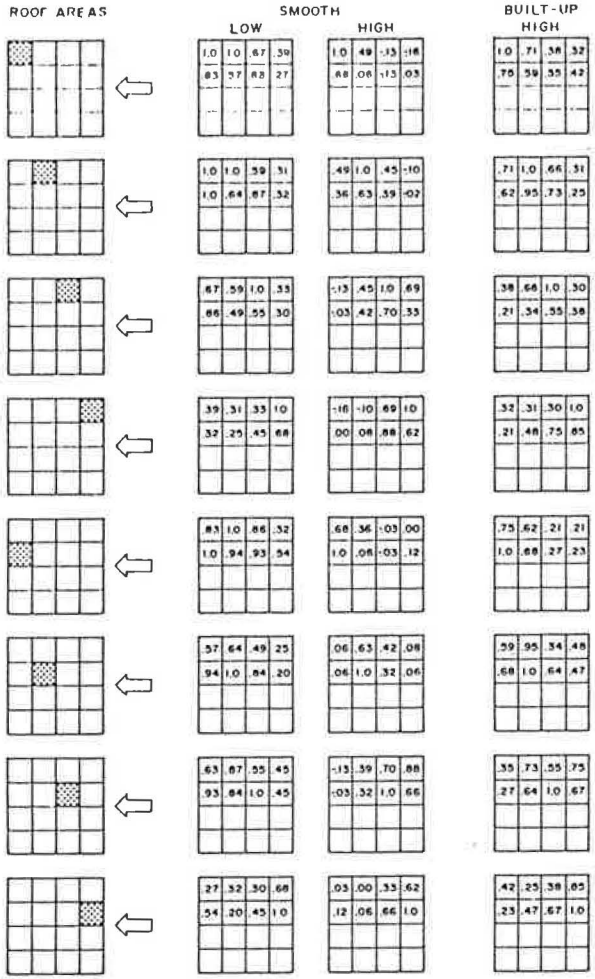

FIG. 10.—Pressure Correlation Coefficients for Various Roof Regions

that two other energy peaks become more pronounced towards the downwind side of the roof, reaching their maximum value in the wake region. The highest of these energy peaks is centered on ~3 Hz ($fh/\bar{V} \approx 0.01$) for the low and ~40 Hz ($fh/\bar{V} \sim 0.45$) for the high model (model scale frequencies). Whereas the response to the gustiness of the wind can be seen over the entire roof on the low model, it only affects the first windward zone of the high model.

This may be due to the greater displacement of the shear layer above the higher model.

Since the effective pressures acting on the subregions of the roof retain a considerable amount of the dynamic nature of the point pressures, it is necessary to define the cross correlations or cross spectra between different roof areas in order to determine the unsteady load acting on still larger parts of the structural system of the roof extending over more than 1/16 of the area. The effectiveness of the dynamic wind loads experienced by large structural elements is thus further reduced. The loss of correlation between two points, which is beneficial for the roof loading, depends on their position and the distance between them.

Correlation coefficients between the area loads on the different regions of the low and high roof are shown in Fig. 10 for different exposures and normal wind. Each zone of Fig. 10 gives the correlation coefficients between the associated shaded area and all the others. The following observations can be made:

1. The height of the roof and the roughness of the exposure are very important factors in the development of high or low correlations. Negative correlation coefficients have been found only in the case of the high model for the smooth exposure wind and are small. Generally, the correlation coefficients change more rapidly for the higher roof and more gradually for the built-up exposure. This may be due to the larger components of roof load dependent on the wind turbulence in the latter case, partially due to the more severe gustiness, and partially due to the closer proximity of the shear layer to the roof.
2. Although the correlation coefficients are expected to decay with increasing separation between the various subareas (the rate of decrease depending on the position of the two subareas, as related to the wind flow direction), this does not always happen. There are cases in which the correlation of the pressure load is higher with a more remote zone of the roof than with a neighboring region. No clear explanation is available; however in some cases it appears to be associated with the reattachment of the separated shear layer.
3. With respect to the wind flow direction, the correlation coefficients (10) appear higher for regions located in the trace of the vortices developed over the roof for the 45° oblique wind direction.

Results of cross-spectral analysis show that, in most cases, the quad-spectra are insignificant; this implies that the out-of-phase components of the pressure load fluctations are negligible. The co-spectra given in Ref. 10 indicate that the pressure load fluctuations are strongly correlated for small separations; thus the co-spectral densities appear fairly comparable to the power spectral densities for adjacent regions, particularly at low frequencies.

Assessment of Effective Wind Loads on Large Roof Subsections

The spectra of pressure loads acting on the 1/16 sections of the roof were used to derive spectra of the total fluctuating wind force acting on larger sections of the roofs. Results were obtained for sections made up of multiples of the 1/16-square areas under the various conditions of exposure, wind direction, and height of roof (10). Typical cases for force spectra acting on a roof quarter

for an oblique wind and different combinations of height and exposure are presented in Fig. 11. Also shown are mean square effective pressure coefficients, found by numerical integration. These coefficients are of the same form as defined in Fig. 9.

In general, the variance coefficients are smaller for larger areas, although they may be higher for the larger area than for some of their component areas if the larger area includes components on the windward side of the roof. It is also interesting to note that larger spectral peaks appear for the lower roof. No clear explanation of this fact is available at present, but the observation indicates that lower roofs may be more susceptible to resonant effects.

Comparison of Local Pressure Coefficient Results with Codes and Standards

Since pressure coefficients are determined with respect to different reference speeds in various countries, it is very difficult to make comparisons directly between coefficients. Instead, a simple illustrative comparison is made in terms of pressure acting on the roofs of a low and a higher building, similar to those used in this study, according to the specifications of the 1977 Commentary to the National Building Code of Canada (NBCC) (simple method), the American National Standard Institute (ANSI A58.1-1972), and the present results. The comparison in summarized in Fig. 12 which shows both the actual pressures, and ratios normalized by the current experimental results. Ratios greater than 1.0 imply code conservatism. The wind speed considered corresponds to an hourly average of 60 mph at 30 ft over an open country exposure. Considering a similar storm system, i.e., the same gradient height speed over a densely built-up urban environment, the corresponding hourly average speed at 30 ft would be only 23 mph. Since the simple method of the NBCC does not recognize any terrain differences, the same values are specified for both exposures.

The ANSI refers all pressure coefficients to the fastest mile speed at roof height. Conversion of the hourly average of 60 mph to a fastest mile of 77 mph was made by using Hollister's charts (6). Different values of velocity pressures (which include gust effects) are specified for different exposures.

To determine the pressures from the present study, the wind speed at roof height was calculated using the experimental velocity profiles of Fig. 2. The pressure coefficients used from the experimental study are the worst peak suction coefficients measured at any point in the area considered, and thus do not include any alleviation associated with spatial averaging. This comparison was adopted because the areas used in these experiments do not conveniently aline with the divisions of roof areas considered in the NBCC or ANSI standard.

The comparison shows that the NBCC significantly overestimates the pressure loads, in particular for the corner region, the built-up terrain, and the lower building. The results suggest some adjustment should be made for the edge and corner specified coefficients which are very high, and that allowance for a rougher exposure in the simple method of the Canadian Code might be worthwhile. The ANSI also significantly overestimates the negative pressures on the perimeter zones; however the ANSI appears to underestimate some of the local loads in the interior of the roof, particularly for the higher building and the rougher terrain. This is likely to be compensated by spatial averaging as per Figs. 6 and 8.

Examination of the measured pressures reveals that generally the dynamic component predominates. Codes usually overestimate the mean loads and underestimate the gust factors. For example, the NBCC considerably overestimates the mean (by factors of 1.5 and up), whereas the gust factors found experimentally were typically in the range 2–7.5 compared to the value of 2.5

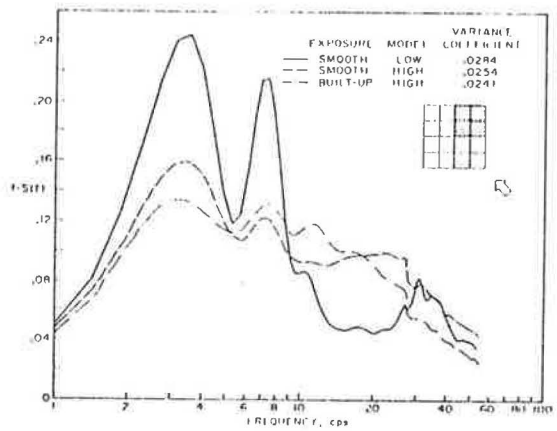

FIG. 11.—Spectra of Pressure Loads Acting on a Roof Quarter

CAVEAT: PRESSURE VALUES DO NOT INCLUDE ANY RESONANT EFFECT

EXPOSURE =		Peak Wind Pressures In psf and As Ratios of Those Found in the Present Study											
		Smooth (NBCC: A; ANSI: C)						Built-up (NBCC: C; ANSI: A)					
REGION =		R		W		C		R		W		C	
		psf	ratio	psf	ratio	psf	ratio	psf	ratio	psf	ratio	psf	ratio
NBCC	Low	-26.7	1.17	-53.2	1.87	-79.7	2.80	-26.7	2.68	-53.2	3.02	-79.7	4.53
	High	-36.2	0.98	-72.5†	1.57†	-109.0†	1.96†	-36.2	1.52	-72.5†	2.67†	-109.0†	3.21†
ANSI	Low	-18.9	0.83	-64.8	2.27	-135.0	4.74	-7.0	0.71	-24.0	1.36	-50.0	2.84
	High	-25.2	0.68	-86.4	1.87	-180.0	3.24	-13.3	0.56	-15.6	1.68	-95.0	2.79
Present Study	Low	-22.8	1.00	-28.5	1.00	-28.5	1.00	-9.9	1.00	-17.6	1.00	-17.6	1.00
	High	-37.0	1.00	-46.2	1.00	-55.5	1.00	-23.8	1.00	-27.2	1.00	-34.0	1.00

Note: 1 psf = 47.9 N/m^2
1 ft. = 305 mm

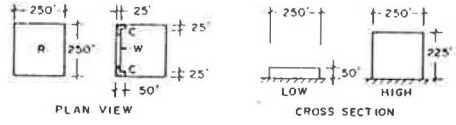

† under the provisions of the 1980 NBCC, for taller buildings the coefficients specified for C are reduced by a factor of 0.67 and for W by a factor of 0.75. Similar reductions have also been effected for low-rise buildings.

FIG. 12.—NBCC, ANSI, and Comparative Experimental Values

specified by the Code. These large experimental gust factors may be particularly significant if the structural response of all or part of the roof is susceptible to dynamic effects. It should be noted that since the experimental coefficients used in the aforementioned comparisons are local values, spatial averaging will further reduce the loads appropriate for overall structural considerations. This

$\bar{V}$ = mean velocity;
V_g = mean wind velocity at gradient height;
Z = height above ground;
Z_o = roughness length;
Z_g = gradient height;
κ = von Karman's constant;
ρ = air density;
σ_p = RMS pressure acting on each square region; and
τ_o = surface shear stress.